DOI: 10.13009/EUCASS2023-094
Aerospace Europe Conference 2023 – 10TH EUCASS – 9TH CEAS

Reduced-Scale Generic Future Fighter Aerodynamic Model Using Neuro-Fuzzy Hybridized with Differential Evolution

Vitor Taha Sant'Ana[1], Roger Larsson[2], Petter Krus[3], Roberto Mendes Finzi Neto[4]
[1] PhD Guest Student at Department of Management and Engineering, Linköping University, 58183 Linköping, Sweden, vitsa83@liu.se
[2] SAAB Aeronautics AB, Linköping, Sweden, roger.gunnar.larsson@saabgroup.com
[3] Department of Management and Engineering, Linköping University, 58183, Linköping, Sweden, petter.krus@liu.se
[4] Laboratory of Mechanical Structures, Universidade Federal de Uberlândia, Uberlândia, Brasil, finzi@ufu.br

Abstract

Accurate aerodynamic modeling is crucial for understanding and optimizing the behavior of aircraft systems. This work presents a novel approach to developing a low-cost yet high-fidelity aerodynamic model using machine learning techniques and experimental flight data from a reduced-scale Generic Future Fighter (GFF). The proposed model leverages Neuro-Fuzzy combined with Differential Evolution for training the acquired data, while employing a Fuzzy Rule-Based System (FRBS) with Gaussian-shaped membership functions for inputs. By effectively predicting forces and moments based on input variable values, the developed model serves as a tool for system identification specific to the aircraft under investigation. The results shows that the Neuro-Fuzzy has a good adaptability to this kind of identifications.

1. Introduction

The usage of artificial intelligence (AI) and machine learning (ML) in the field of aerodynamics predictions started with airfoil lift curve predictions using sparse data and artificial neural networks (ANN) [1] and has been increasingly required through the years. In the present time, there have been a lot of publications using the ML techniques to predict the unsteady aerodynamics model from numerical or experimental data.

The Neuro-Fuzzy technique, based on the literature review, is a good ML technique to predict the unsteady aerodynamics of an aircraft. [2] presented a full aerodynamic model obtained through experimental data of a full-size aircraft using Neuro-Fuzzy and very rich data set, including maneuvers and aleatory deflections of the control surfaces. Also, [3] obtained the stability derivatives of a full-size aircraft using Neuro-Fuzzy with Genetic Algorithms, the training was also performed using experimental data.

In terms of the absence of trustful experimental data, [4] designed a reduced-scale version of Cessna 182 and simulated the remote-controlled aircraft in a flight simulator environment. The authors acquired good results with the numerical data exported from the flight simulator. In addition, the Neuro-Fuzzy with Differential Evolution (NF-DE) behaved with high robustness and good accuracy.

Trusting in the robustness of the NF-DE, this work's main objective is to develop a low-cost (in computational terms) yet high-fidelity aerodynamic model using experimental flight data from a reduced-scale Generic Future Fighter (GFF). Such a model has the potential to reduce the reliance on expensive and time-consuming physical experiments or even CFD simulations, which consume several times for a large flight envelope, allowing for more efficient design iterations and performance evaluations. Additionally, the proposed model can serve as a valuable tool for system identification, accurately describing the behavior of the GFF based on input variable values. The exploration of potential applications, such as the development of a reduced-scale flight test simulator for new fighters, further underscores the practical significance of this research.

The aim is to capture the flight mechanics of the GFF and create an accurate model that can predict forces and moments for the aircraft. This research endeavors to contribute to the advancement of aerodynamic modelling techniques, providing valuable insights for aircraft design and simulation.

DOI: 10.13009/EUCASS2023-094

2. Methodology

This section describes the fuzzy rule-based systems (FRBS), the Neuro-Fuzzy architecture, and the GFF's non-inertial body-axis flight dynamics.

2.1 Fuzzy Rule Based System

The FRBS contains four components: the input processor, the rule bases, the inference machine, and the output processor [5]. These components can be seen in Figure 1, and their description are listed below.

Input processor – The input processor converts real numbers into fuzzy sets with a degree of membership. This process is also known as fuzzification.

Rule bases – The rule bases within the Fuzzy Rule-Based System (FRBS) can be seen as linguistic interpretations of the system behavior, forming the core of the FRBS. There rule bases are created based on specialist knowledge using IF...THEN type prepositions. This crucial step establish the relationships between the linguistic variables. Allowing for the interpretation and reasoning of the system outputs based on the inputs.

Inference machine – The inference machine establishes the correlation between the input fuzzy sets with the output fuzzy functions (Takagi-Sugeno method), and the association is oriented by the rule bases.

Output processor – The output processor performs the defuzzification, which is the process of converting the value of the output functions back into real numbers through a weight pondered equation.

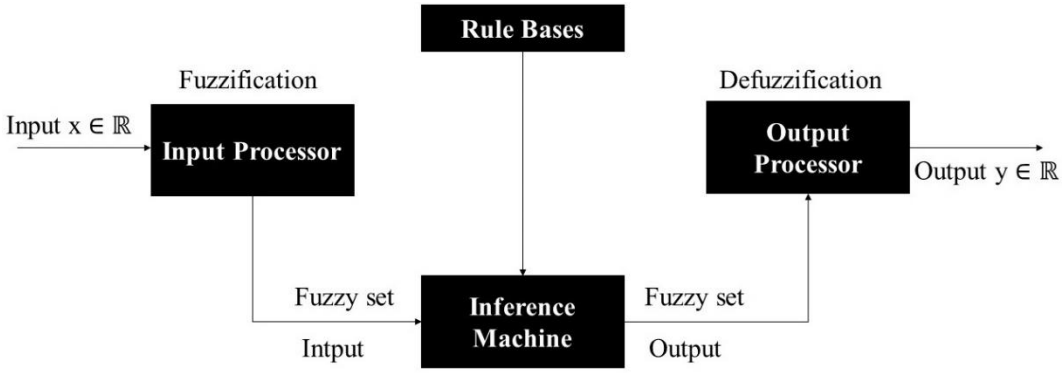

Figure 1 - FRBS architecture

This work used the Takagi-Sugeno (TS) inference method in the FRBS to train the Neuro-Fuzzy. This inference method manages the output as functions dependent on the input variables. These output functions incorporate parameters that serve as multipliers for the input variables. By adjusting these parameters, the TS method allows for fine-tuning and customization of the output functions to accurately represent the relationship between the inputs and outputs, resulting in precise and tailored modelling of the system behavior.

To better describe the TS inference method, the two following rules are proposed [5]. The architecture of TS inference method is shown in Figure 2.

Rule 1: If (X is A_1 AND Y is B_1) THEN (Z is z_1)

Rule 2: If (X is A_2 AND Y is B_2) THEN (Z is z_2)

DOI: 10.13009/EUCASS2023-094

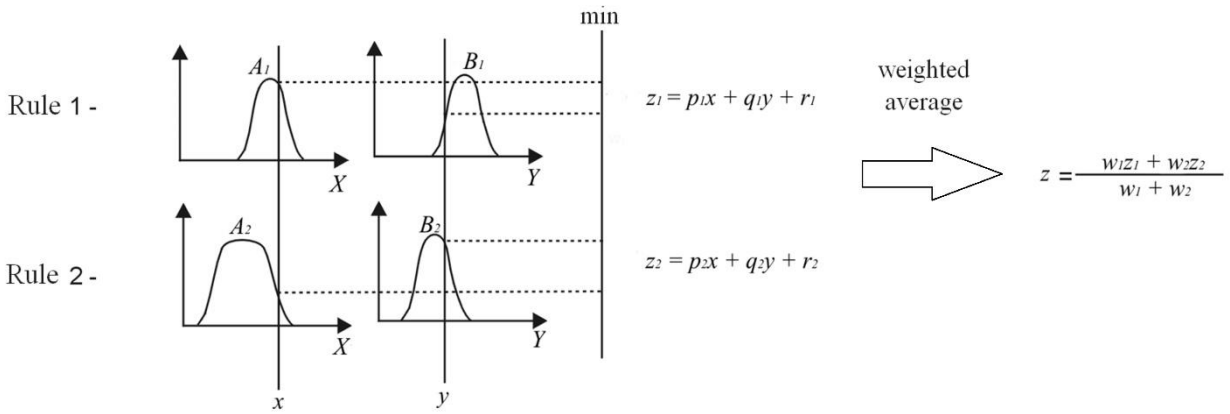

Figure 2 - Takagi-Sugeno inference method

2.2 Neuro-Fuzzy

The Neuro-Fuzzy is a ML technique which combines the interpretability of the FRBS with the adaptability of the ANN [6]. The architecture of the Neuro-Fuzzy with the description of each layer responsibility is described below.

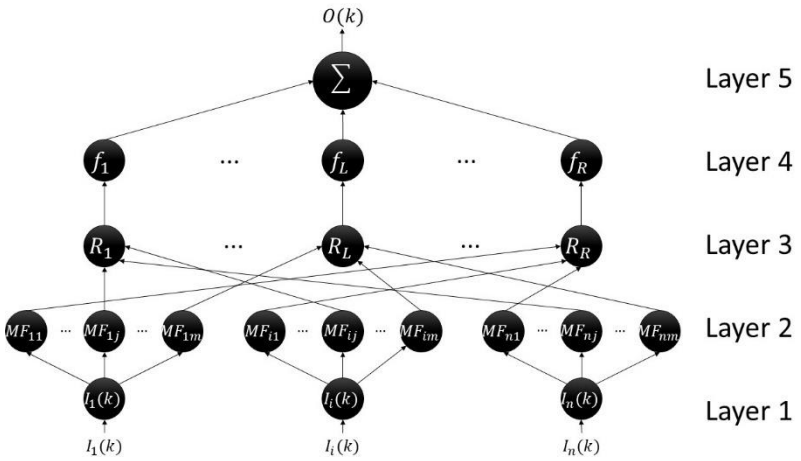

Figure 3 - Neuro-Fuzzy architecture

The Neuro-Fuzzy architecture counts with five layers, which can be described as:

Layer one: Each node in this layer receives a single input variable $I_i(k)$ for the training process. The output of the i_{th} node in the first layer at time k, denoted as $u_i^{(1)}(k)$, is equal to the input variable $I_i(k)$.

$$u_i^{(1)}(k) = I_i(k) \tag{1}$$

Layer two: In this layer the fuzzification of input variables is performed, that is, the real numbers are transformed into Fuzzy subsets with a certain degree of pertinence. The membership functions (MF) are built for the description of the inputs. Considering that the membership functions are approximated by Gaussian functions, the output of node ij from layer 2 at time k, $u_{ij}^{(2)}(k)$, is given by:

$$u_{ij}^{(2)}(k) = e^{-\frac{\left(u_i^{(1)}(k) - m_{ij}(k)\right)^2}{2\sigma_{ij}^2(k)}} \tag{2}$$

Layer three: The rule bases consist of prepositions of the type IF…THEN…, forming the correlation between input sets and output functions of the Adaptive Neuro-Fuzzy Inference Systems (ANFIS). For each rule, the logical operator AND and OR are applied, which corresponds to the minimum and maximum respectively. The output from the L node of the third layer ($u_L^{(3)}(k)$) is a function of the layer 2 for the selected output from rule R_L.

DOI: 10.13009/EUCASS2023-094

Layer four: The nodes from this layer are known as consequent nodes, and they are defined as a function (output function) $f_L: R^n \rightarrow R$ in which $f_L = f(I_1, \dots, I_i, \dots, I_n, w_{1L}, \dots, w_{jL}, \dots, w_{oL}, k)$, where $w_{1L}, \dots, w_{oL}$ are weights that are determined in the ANFIS training optimization. Thereby, the output from node L of the fourth layer, $u_L^{(4)}(k)$, is calculated as:

$$u_L^{(4)} = u_L^{(3)}(k) f_L(I_1, \dots, I_i, \dots, I_n, w_{1L}, \dots, w_{jL}, \dots, w_{oL}, k) \tag{3}$$

Layer five: The last layer is responsible for providing the ANFIS result, through a pondered weight estimation given by the following equation:

$$O(k) = -\frac{\sum_{L=1}^{R} u_L^{(4)}(k)}{\sum_{L=1}^{R} u_L^{(3)}(k)} \tag{4}$$

2.3 Differential Evolution

The differential evolution (DE) is used to optimize the Neuro-Fuzzy parameters, which are the mean and standard deviations from the membership functions used to model the input variables, and the output functions.

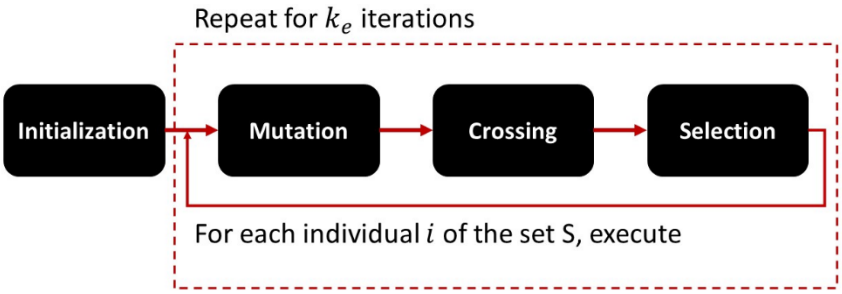

Figure 4 - Differential evolution scheme representation

The parameters for the DE are shown in Table 1. The training time takes around 4-5 hours to be complete using the parameters presented below.

Table 1 - Differential evolution parameters

Parameter	Value
Number of individuals	150
Number of variables	25
Crossing probability	0.95
Mutation probability	0.4

2.4 GFF flight dynamics

The Generic Future Fighter (GFF) is a 13% scale representation of a 5th generation fighter, and conceptual design was developed by SAAB aeronautics. The subscale aircraft was built by Linköping University [7]. For this aircraft, [8] created a low-cost instrumentation to acquire the aerodynamic data through experimental flights. The aircraft is equipped with onboard devices, e.g., Pixhawk, which records the acceleration, the attitude angles rate, the velocity, the sideslip angle, the angle of attack, and more. The Figure 5 shows the 6 degrees of freedom (DOF) from the reduced scale GFF.

According to [9], the forces that acts in the non-inertial body axes of the aircraft can be obtained with the Equations 5, 6 and 7.

DOI: 10.13009/EUCASS2023-094

$$a_{X_{cg}} = \frac{X}{m} = \left(\dot{U} + QW - RV + g\sin\theta\right) \tag{5}$$

$$a_{Y_{cg}} = \frac{Y}{m} = \left(\dot{V} + UR - WP - g\cos\theta\sin\phi\right) \tag{6}$$

$$a_{Z_{cg}} = \frac{Z}{m} = \left(\dot{W} + VP - QU - g\cos\theta\cos\phi\right) \tag{7}$$

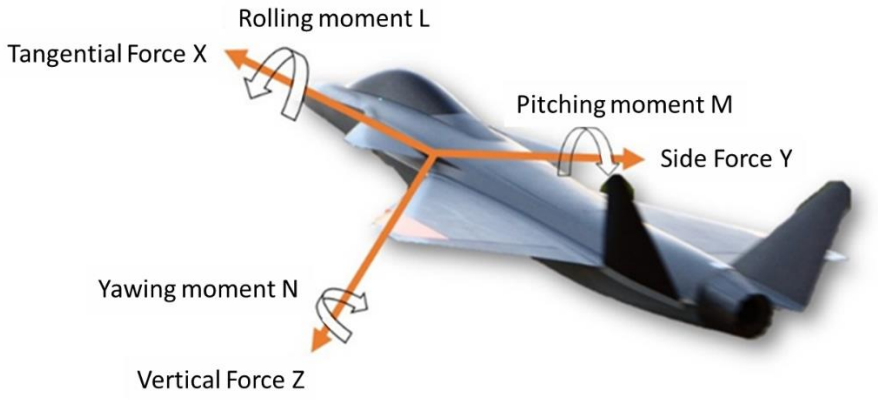

Figure 5 - GFF 6 DOF

The moments around the non-inertial body axes, depends on the derivative of the roll, pitch, yaw, and the inertial moments. The moments that act in the GFF's center of gravity can be described in Equations 8, 9 and 10, according to [7].

$$L = I_{XX}\dot{P} - I_{XZ}\left(\dot{R} + PQ\right) + (I_{ZZ} - I_{YY})QR \tag{8}$$

$$M = I_{YY}\dot{Q} + I_{XZ}(P^2 - R^2) + (I_{XX} - I_{ZZ})PR \tag{9}$$

$$N = I_{ZZ}\dot{R} - I_{XZ}\dot{P} + (I_{YY} - I_{XX})PQ + I_{XZ}QR \tag{10}$$

Where I_{XX}, I_{YY}, I_{ZZ} are the inertial moments and I_{XZ} is the product of inertia, which is equal 0 for this aircraft. The inertial moments values are 0.56, 5.28 and 5.56, respectively. Also P is the roll rate, Q is the pitch rate and R is the yaw rate.

3. Results

This section is going to present the aerodynamic model for each DOF of the GFF obtained with the Neuro-Fuzzy. The training and validation graphs are going to be presented. For the training and validation 35,000 and 11,000 data points have been used respectively. To evaluate the accuracy of the trainings and validations, the coefficient of determination (R^2) is applied.

The input variables were adjusted and scaled to a normalized range of 0 to 1. This normalization facilitated the process of modifying the input variables when necessary, as they were now represented within a standardized and consistent range.

3.1 Longitudinal

The longitudinal forces and moments are the force in X-axis, the force in Z-axis, and the moment around Y-axis (pitch moment M).

3.1.1 Force X

DOI: 10.13009/EUCASS2023-094

The force X coefficient is calculated with Equation 5, where T is the thrust of the GFF. The training and validation graph can be observed in Figure 6. The coefficient of determination for the training is 44%, and for validation is 46%.

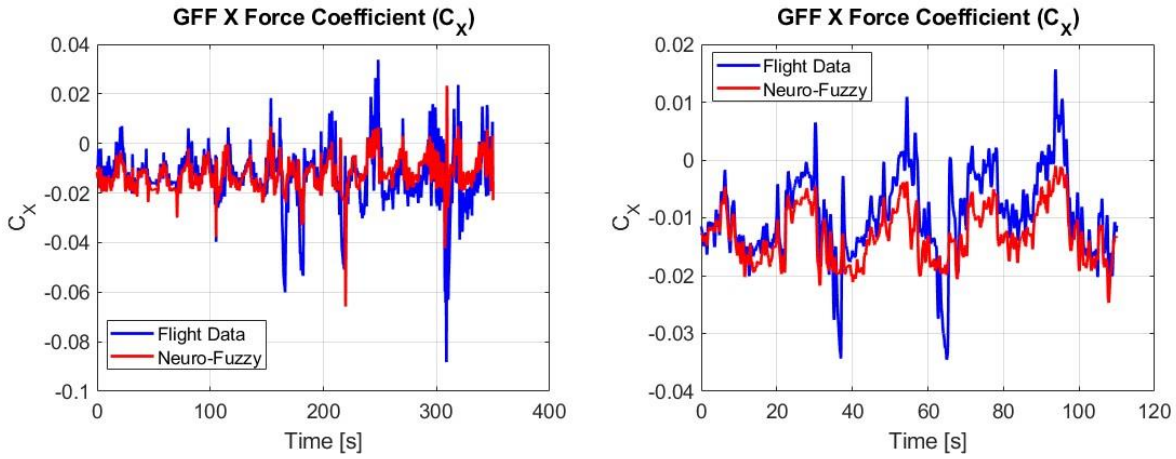

Figure 6 - X force coefficient

After accomplishing the training, the input membership functions parameters are available and illustrated in Figure 7. Table 2 is presenting the membership functions parameters for the angle of attack, the elevator deflection, and the pitching rate. Also, the Table 3 shows the output constant functions optimized for C_X.

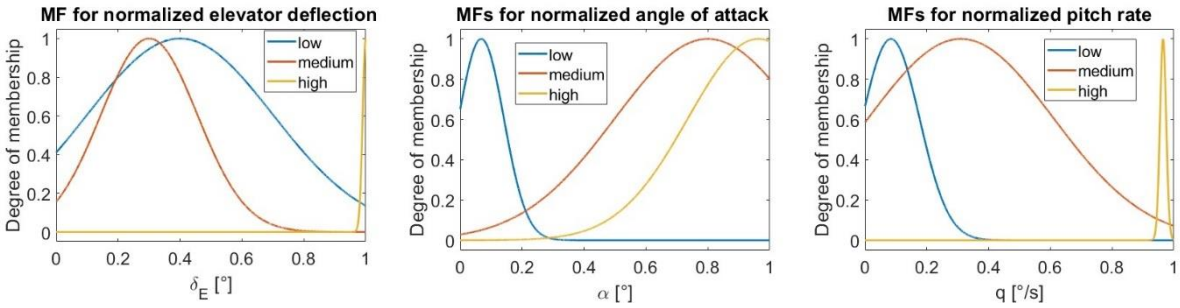

Figure 7 - Membership functions for the input variables of C_X

Table 2 – Means and standard deviations for the input membership functions referred to C_X

	Mean	**Standard deviation**
α	(0.0677 0.8000 0.9629)	(0.0731 0.3000 0.2270)
δ_E	(0.4000 0.3000 1.0000)	(0.3000 0.1559 0.0100)
q	(0.0835 0.3102 0.9651)	(0.0927 0.3000 0.0100)

Table 3 - Optimized outputs for X force coefficient

Output	**Consequent**
C_X	(-0.0737 -0.0800 -0.0300 -0.0382 -0.0151 0.0300 0.0400)

The stability derivatives for the tangential force coefficient can be observed in Figure 8. The most influent variable for this force is the angle of attack.

DOI: 10.13009/EUCASS2023-094

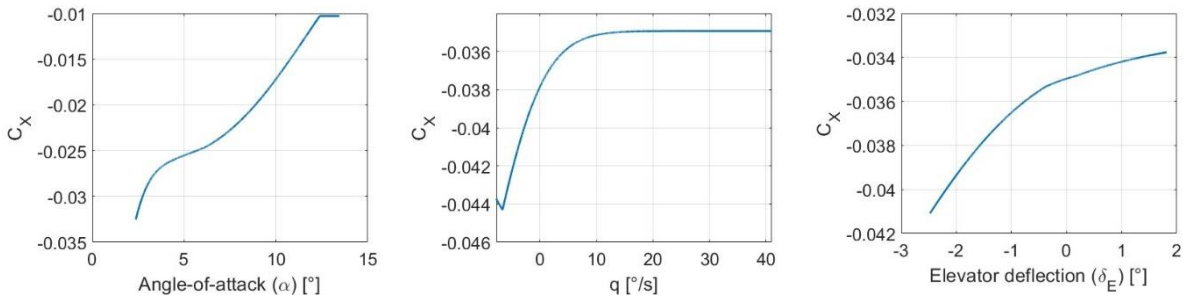

Figure 8 - Stability derivatives for C_X

3.1.2 Pitch Moment

The pitch moment is calculated using the Equation 9, and the input variables used to model this moment coefficient aerodynamically were: elevator deflection, aileron deflection and angle of attack rate. The coefficient of determination for the training is 60% and for validation is 44%. The Figure 9 shows the training and validation graphs.

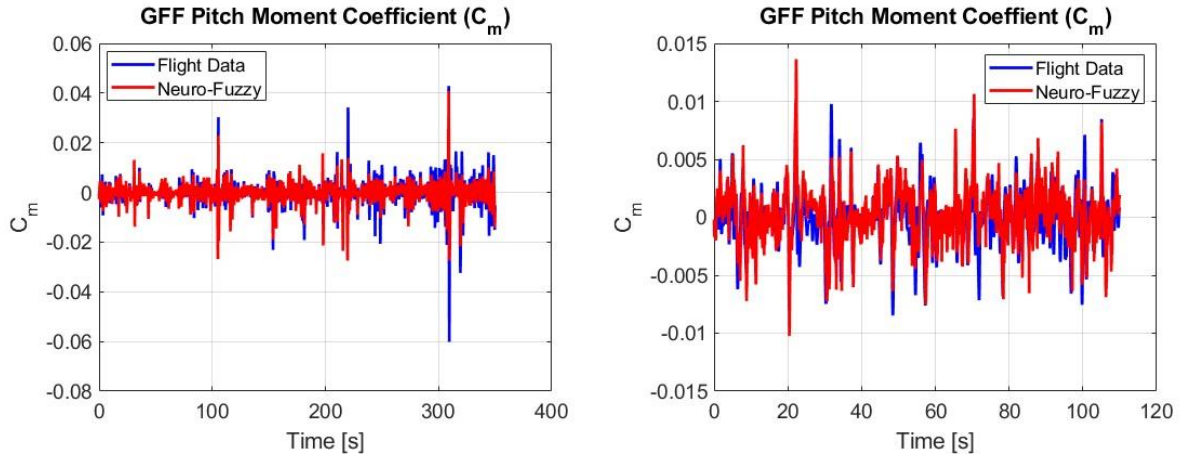

Figure 9 - Pitch moment coefficient

The shape of the input's membership functions can be observed in Figure 10, while the parameters from the MF are shown in Table 4. The output values for the seven constant functions are illustrated in Table 5.

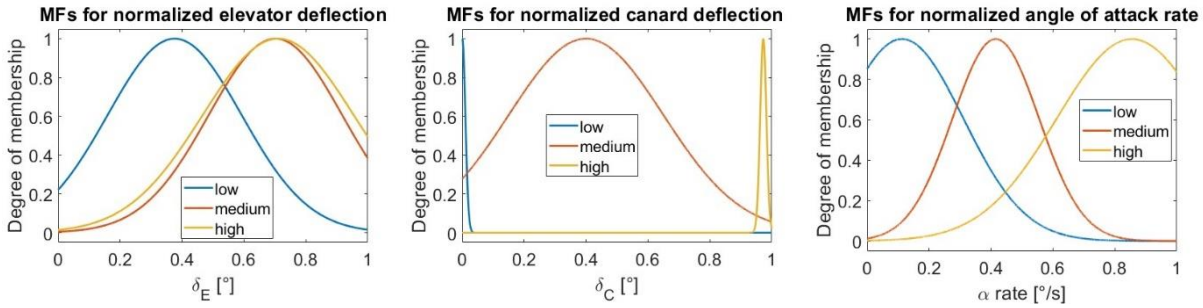

Figure 10 - Membership functions for the input variables of C_m

Table 4 - Means and standard deviations for the input membership functions referred to C_m

	Mean	Standard deviation
δ_E	(0.3760 0.7017 0.7106)	(0.2166 0.2156 0.2439)
δ_C	(0.0000 0.4000 0.9726)	(0.0100 0.2500 0.0100)
$\dot{\alpha}$	(0.1121 0.4152 0.8551)	(0.1986 0.1401 0.2430)

DOI: 10.13009/EUCASS2023-094

Table 5 - Optimized output functions for pitch moment coefficient

Output	Consequent
C_m	(-0.040 -0.0493 -0.0137 0.0200 0.0112 0.0277 0.0458)

The stability derivatives for the pitch moment coefficient are presented in Figure 11. The most influential variable is the elevator deflection. The canard deflection is linked to the elevator deflection, and it is inversely proportional to that.

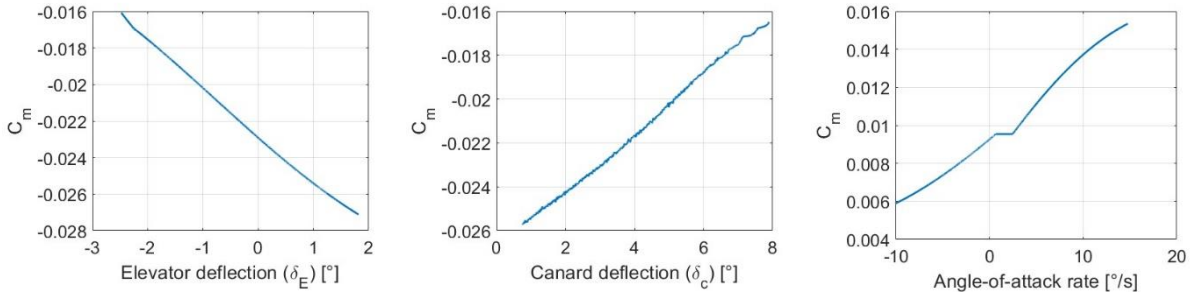

Figure 11 - Stability derivatives for C_m

3.1.3 Force Z

The force coefficient in Z-axis is the most accurate degree of freedom. The input variables are the same used to train the C_X, which are: angle of attack, elevator deflection and pitching rate. The coefficient of determination for the training is 96% and for validation is 88%. The Figure 12 shows the training and validation graphs.

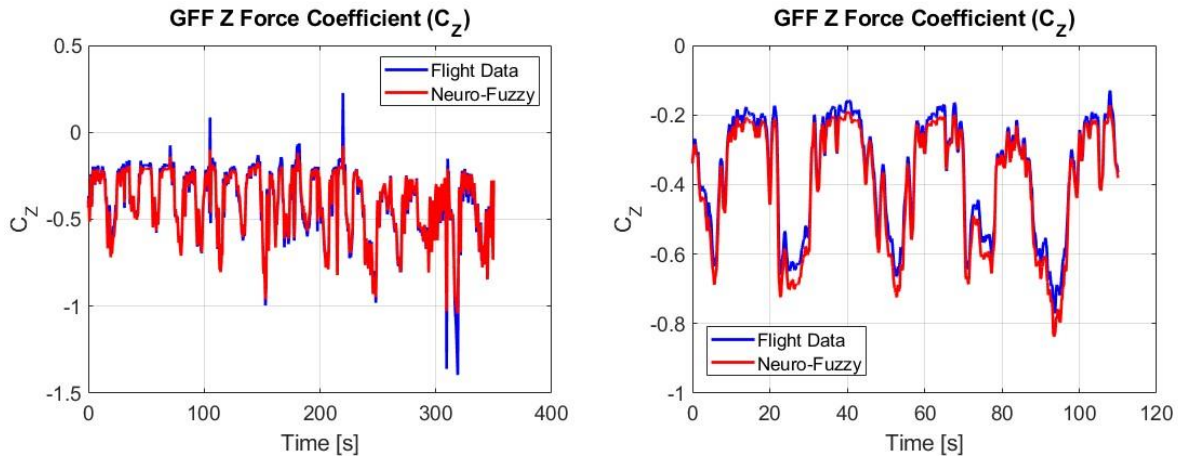

Figure 12 - Z force coefficient

The membership functions for the three input variables can be observed in Figure 13. The parameters used to build the Gaussian functions are shown in Table 6.

DOI: 10.13009/EUCASS2023-094

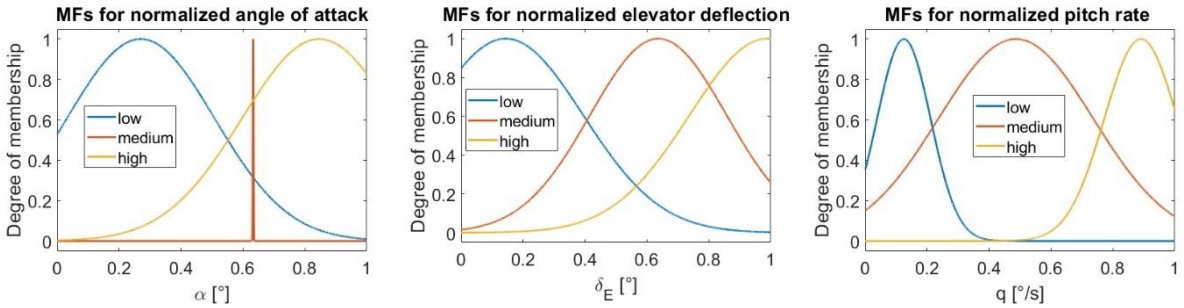

Figure 13 - Membership functions for the input variables of C_Z

Table 6 - Means and standard deviations for the input membership functions referred to C_Z

	Mean	Standard deviation
α	(0.2697 0.6329 0.8465)	(0.2389 0.0000 0.2500)
δ_E	(0.1437 0.6366 0.9877)	(0.2500 0.2205 0.2500)
q	(0.1246 0.4866 0.8905)	(0.0864 0.2500 0.1182)

The constant functions for the C_Z is shown in Table 7.

Table 7 - Optimized output functions for Z force coefficient

Output	Consequent
C_Z	(-1.2157 -1.0222 -1.1000 -0.9000 -0.2054 -0.0343)

The stability derivatives for the vertical force coefficient is presented in Figure 14.

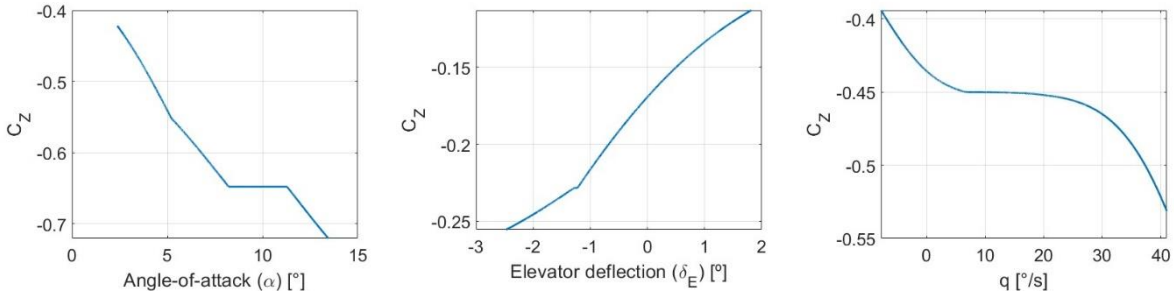

Figure 14 - Stability derivatives for C_Z

In conclusion, the stability derivatives in the longitudinal axes unequivocally demonstrate that the angle of attack is the most critical variable, followed by the elevator deflection and the pitching rate.

3.2 Lateral-Directional

The lateral-directional encompass the force in Y-axis, the moment around X-axis (roll moment L), and the moment around Z-axis (yaw moment R).

3.2.1 Roll Moment

The roll moment coefficient is a little tricky to guarantee a good training, especially for aircrafts with low inertia moments like the GFF. To achieve a reasonable fit, three input variables was used: sideslip angle, sideslip angle rate and aileron deflection. The coefficient of determination for the training is 31%, which is a low R^2. However, for the validation is 41%. The Figure 15 presents the training graph (on the left side) and the validation graph (on the right side).

DOI: 10.13009/EUCASS2023-094

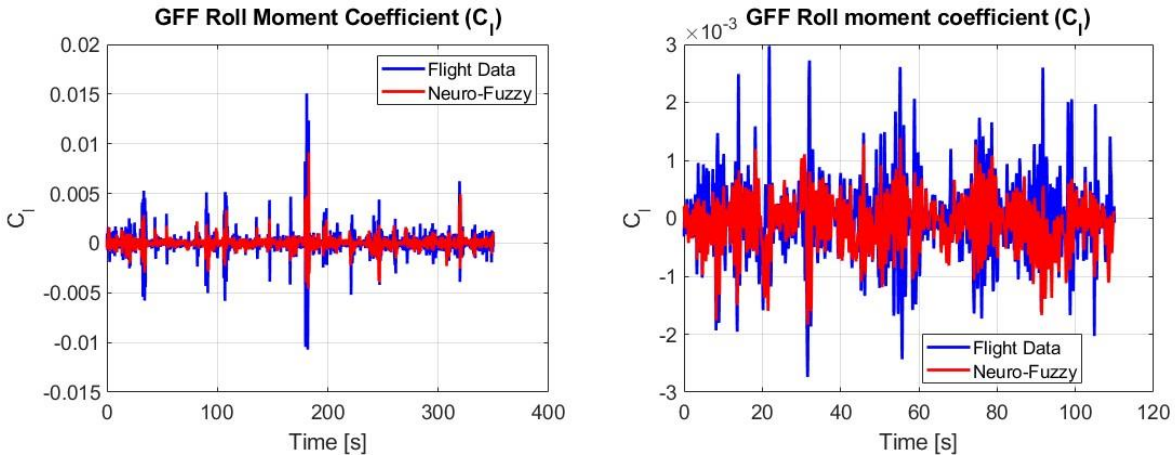

Figure 15 - Roll moment coefficient

The membership functions for the three input variables can be seen in Figure 16, and the parameters from these MFs are presented in Table 8. Table 9 shows the output variables for the seven consequent functions.

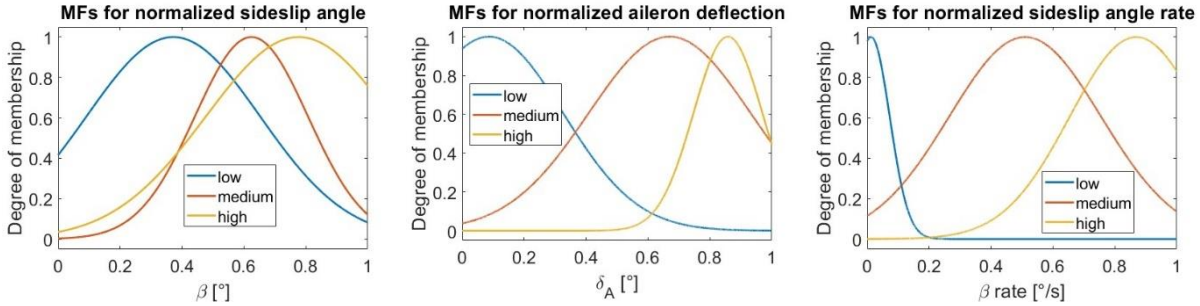

Figure 16 - Membership functions for the input variables of C_l

Table 8 - Means and standard deviations for the input membership functions referred to C_l

	Mean	**Standard deviation**
β	(0.3717 0.6241 0.7766)	(0.2809 0.1829 0.3000)
$\dot{\beta}$	(0.0121 0.5100 0.8690)	(0.0604 0.2453 0.2147)
δ_A	(0.0860 0.6701 0.8584)	(0.2397 0.2615 0.1113)

Table 9 - Optimized output functions for roll moment coefficient

Output	**Consequent**
C_l	(-0.0104 -0.0063 -0.0008 0.0008 0.0042 0.0119 0.0128)

The stability derivatives for the roll moment coefficient can be seen in Figure 17 below. The sideslip angle has a crucial influence in the prediction of C_l.

DOI: 10.13009/EUCASS2023-094

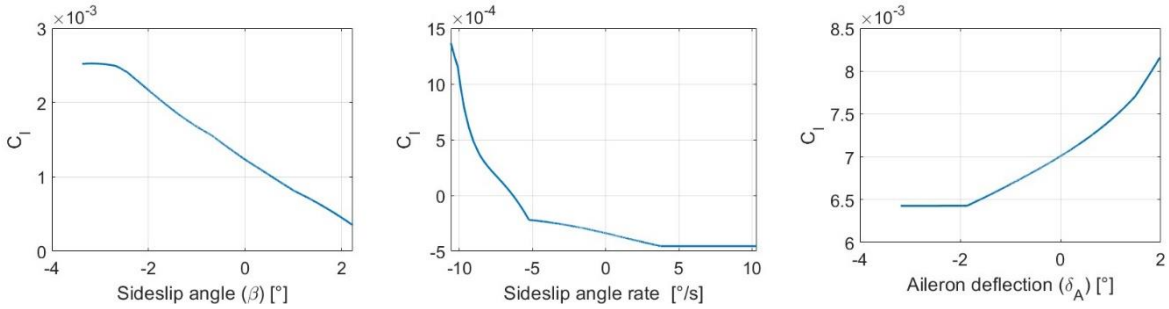

Figure 17 - Stability derivatives for C_l

3.2.2 Force Y

The force in the Y-axis has three input parameters, which are: sideslip angle, angle of attack, and sideslip angle rate. The accuracy of the aerodynamic model is measured with the coefficient of determination, and in this case the value is 64% for the training, and 76% for the validation data set. The training and validation graph are presented in Figure 18. The membership functions shape used to describe the fuzzy sets of the input variables are Gaussians, and they are illustrated in Figure 19.

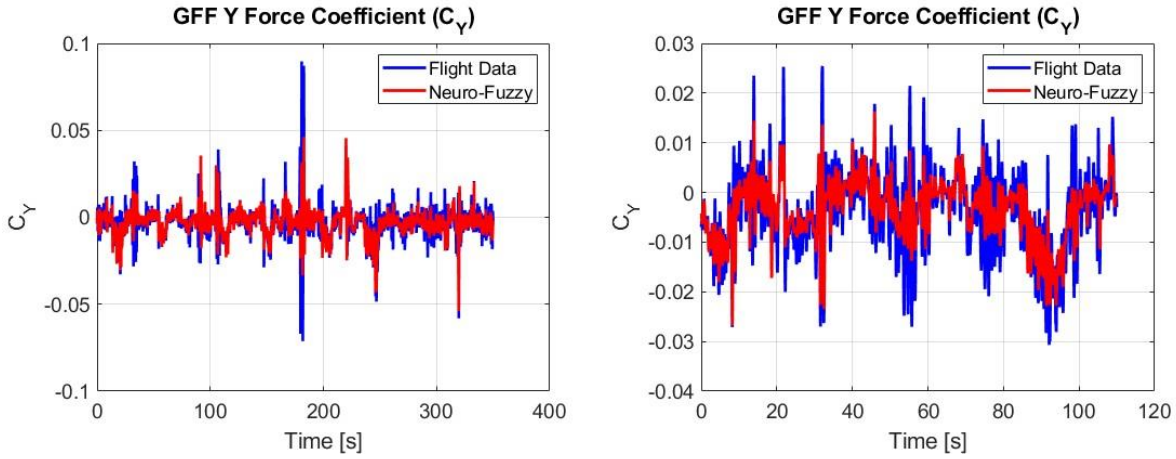

Figure 18 - Y force coefficient

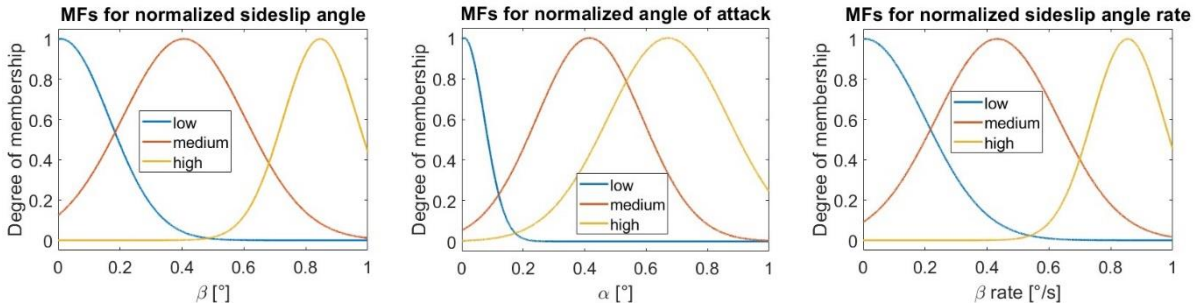

Figure 19 - Membership functions for the input variables of C_Y

The parameters of the Gaussian functions for the three input variables used to model the Y-axis force coefficient are presented in Table 10.

DOI: 10.13009/EUCASS2023-094

Table 10 - Means and standard deviations for the input membership functions referred to C_Y

	Mean	Standard deviation
β	(0.0084 0.4054 0.8465)	(0.1566 0.1986 0.1198)
α	(0.0075 0.4156 0.6713)	(0.0657 0.1723 0.1961)
$\dot{\beta}$	(0.0051 0.4328 0.8548)	(0.1942 0.1974 0.1154)

The output functions are modelled as constant parameters, and they are presented in the Table 11 below.

Table 11 - Optimized output functions for Y force coefficient

Output	Consequent
C_Y	(-0.0725 -0.0281 -0.0178 0.0024 0.0217 0.0694 0.0666)

The stability derivatives for the side force coefficient are presented in Figure 20. There is a slight difference between the influences in this case, and the sideslip angle seems to be the most influent input variable in this case.

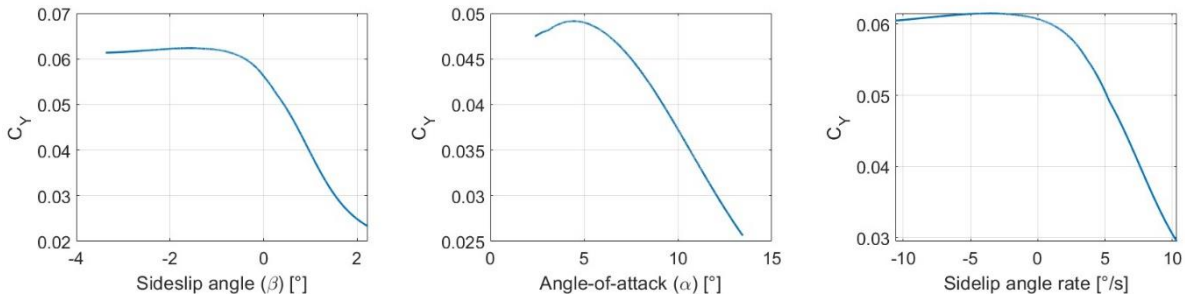

Figure 20 - Stability derivatives for C_Y

3.2.3 Yaw Moment

The yaw moment is the moment around the Z-axis of the non-inertial body axis of any aircraft. In this study, the input variables used to model this moment are aileron deflection, rolling rate and sideslip angle rate. The accuracy for the training data set is 80%, and for the validation data set is 74%. The training graph and the validation graph can be observed in Figure 21. The membership functions for the input variables are presented in Figure 22.

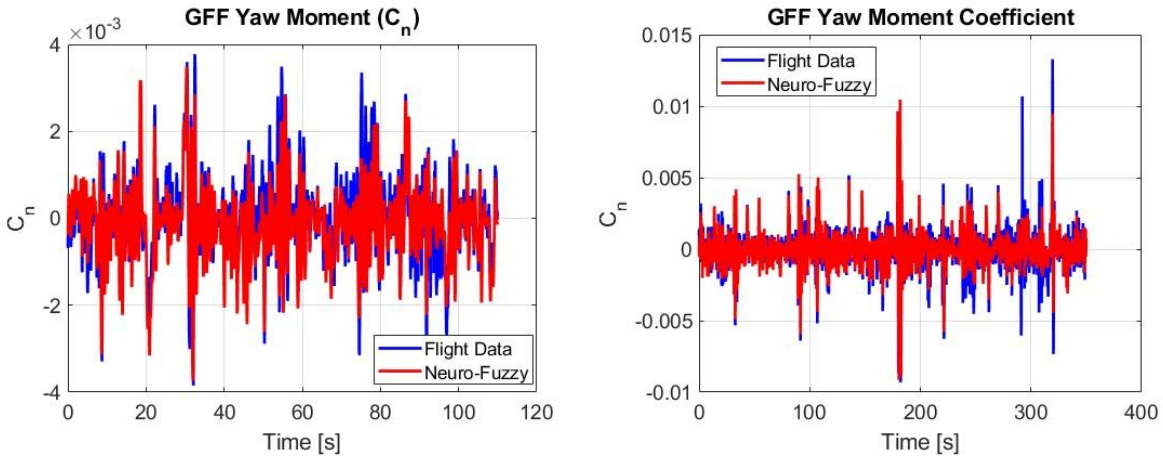

Figure 21 - Yaw moment coefficient

DOI: 10.13009/EUCASS2023-094

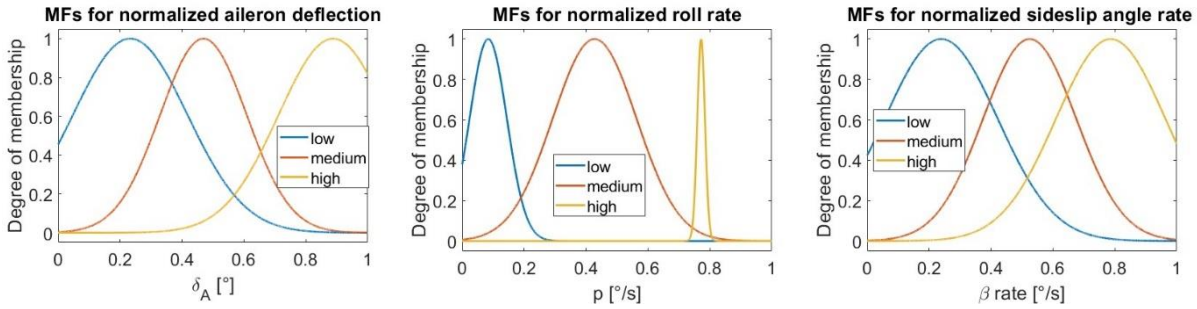

Figure 22 - Membership functions for the input variables of C_n

The means and standard deviations for all the nine membership functions of the input variables are presented in the Table 12.

Table 12 - Means and standard deviations for the input membership functions referred to C_n

	Mean	**Standard deviation**
δ_A	(0.2325 0.4690 0.8880)	(0.1854 0.1401 0.1764)
p	(0.0839 0.4276 0.7718)	(0.0603 0.1355 0.0124)
$\dot{\beta}$	(0.2388 0.5274 0.7865)	(0.1824 0.1504 0.1765)

At least, the coefficients from the seven output functions optimized for the C_n can be observed in Table 13.

Table 13 - Optimized output functions for yaw moment coefficient

Output	**Consequent**
C_n	(-0.0099 -0.0079 -0.0017 0.0019 0.0061 0.0099 0.0130)

The stability derivatives for the yaw moment coefficient are shown in Figure 23. The roll rate does not have a crucial effect on the validation data set. The aileron deflection and the sideslip angle rate are essential for predicting the C_n.

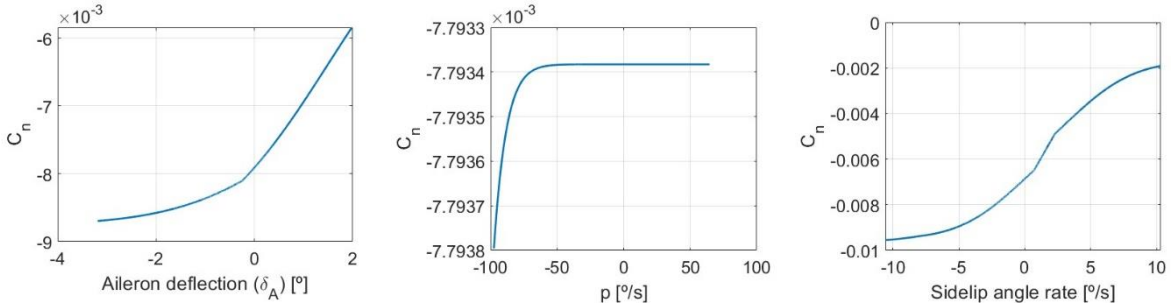

Figure 23 - Stability derivatives for C_n

All the validations are calculated between 80 to 110 milliseconds, which makes this approach a fast model and simulation tool. However, the training time requires to be analyzed on ground, due to fact that the training time needs between 3 to 5 hours to be completed.

This chapter presented all the training and validation graphs for the 6 DOF of the GFF, followed by the membership functions shapes and parameters of all input variables. The results also presented the seven consequent functions for every force and moment.

DOI: 10.13009/EUCASS2023-094

4. Conclusion

This study presented a machine learning technique able to understand and model the dynamic of a reduced scale RC piloted aircraft. The results certify that the Neuro-Fuzzy can be applied in the unsteady aerodynamic model acquisition.

The force coefficient in the X-axis does not perform a good training and a good validation due the fact of the uncertainties of the trust approximation from the GFF. It is a little tricky to predict with high precision the value of the reduced scale ram jet used in the subscale aircraft.

The pitch moment provides a good training, with 60% accuracy. However, the validation accuracy is low, which means that the validation set could be influenced by wind perturbations that were captured by the sensors, which has no correlation with input variables.

The roll moment is the most difficult parameter to model in the GFF's case. It happens because the inertia moment around X-axis (I_{XX}) is very low, equal to 0.56. This maybe explain the very low correlation between the moment and its input variables, most of the time the aircraft is being perturbed by the wind speed instead of the control surfaces or the attitude angles.

The Z-force coefficient, the yaw moment coefficient and the Y-force coefficient has a good correlation coefficient for the training and for the validation, although they can be improved more by adding one or two input variables. However, the computation cost will be increased, which requires a better computer to perform the training.

References

[1] Rajkumar, T., J.E. Bardina. 2002 Prediction of aerodynamic coefficients using neural networks for sparse data. In *FLAIRS Conference* (pp. 242-246).

[2] Brandon, J. M., E. A. Morelli. 2016 Real-time onboard global nonlinear aerodynamic modelling from flight data. *Journal of Aircraft*, *53*(5), 1261-1297.

[3] Roy, A. G., N. K. Peyada. 2017. Longitudinal aircraft parameter estimation using neuro-fuzzy and genetic algorithm based method. In *AIAA Atmospheric Flight Mechanics Conference* (p. 3896).

[4] Sant'Ana, V., I. Staack, R. M. Finzi Neto. 2022 Lateral-directional aerodynamic modeling for numerical results using Neuro-Fuzzy with Differential Evolution. In *33rd International Congress of the Aeronautical Sciences*, Stockholm, 2022. ICAS.

[5] da Motta Jafelice, R. S. 2003. Modelagem fuzzy para dinamica de transferéncia de soropositivos para HIV em doença plenamente manifesta. PhD Thesis. Universidade de Campinas.

[6] Sun, C-T., and J-S. Jang. 1993 A neuro-fuzzy classifier and its applications. In *[Proceedings 1993] Second IEEE International Conference on Fuzzy Systems*, pp. 94-98.

[7] Jouannet, C., P. Berry, T. Melin, K. Amadori, D. Lundström, I. Staack. (2012). Subscale flight testing used in conceptual design. *Aircraft Engineering and Aerospace Technology*, *84*(3), 192-199.

[8] Sobron, A., D. Lundström, I. Staack, P, Krus. (2016). Design and testing of a low-cost flight control and data acquisition system for unstable subscale aircraft. In *30th Congress of The International Council of the Aeronautical Sciences (ICAS), Daejeon, Korea, September 25-30, Daejeon, South Korea.*

[9] Fossen, T. I. (2011). Mathematical models for control of aircraft and satellites. Department of Engineering Cybernetics Norwegian University of Science and Technology, 54-58.